crystals

MDPI

Article

Copper Oxide/Functionalized Graphene Hybrid Nanostructures for Room Temperature Gas Sensing Applications

Monika Gupta [1,2,*], Huzein Fahmi Hawari [1,2,*], Pradeep Kumar [1,2] and Zainal Arif Burhanudin [1,2]

[1] Department of Electrical and Electronic Engineering, Universiti Teknologi PETRONAS, Seri Iskandar 32610, Malaysia; pradeep.hitesh@gmail.com (P.K.); zainalarif.burhanudin@utp.edu.my (Z.A.B.)
[2] Center of Innovative Nanostructures and Nanodevices (COINN), Universiti Teknologi PETRONAS, Seri Iskandar 32610, Malaysia
* Correspondence: monika_18000995@utp.edu.my (M.G.); huzeinfahmi.hawari@utp.edu.my (H.F.H.)

Abstract: Oxide semiconductors are conventionally used as sensing materials in gas sensors, however, there are limitations on the detection of gases at room temperature (RT). In this work, a hybrid of copper oxide (CuO) with functionalized graphene (rGO) is proposed to achieve gas sensing at RT. The combination of a high surface area and the presence of many functional groups in the CuO/rGO hybrid material makes it highly sensitive for gas absorption and desorption. To prepare the hybrid material, a copper oxide suspension synthesized using a copper acetate precursor is added to a graphene oxide solution during its reduction using ascorbic acid. Material properties of the CuO/rGO hybrid and its drop-casted thin-films are investigated using Raman, FTIR, SEM, TEM, and four-point probe measurement systems. We found that the hybrid material was enriched with oxygen functional groups (OFGs) and defective sites, along with good electrical conductivity (Sheet resistance~1.5 kΩ/□). The fabricated QCM (quartz crystal microbalance) sensor with a thin layer of the CuO/rGO hybrid demonstrated a high sensing response which was twice the response of the rGO-based sensor for CO_2 gas at RT. We believe that the CuO/rGO hybrid is highly suitable for existing and future gas sensors used for domestic and industrial safety.

Keywords: sensing materials; CuO/rGO hybrid; graphene; QCM; gas sensor; room temperature sensing

check for updates

Citation: Gupta, M.; Hawari, H.F.; Kumar, P.; Burhanudin, Z.A. Copper Oxide/Functionalized Graphene Hybrid Nanostructures for Room Temperature Gas Sensing Applications. *Crystals* **2022**, *12*, 264. https://doi.org/10.3390/cryst12020264

Academic Editors: Rabindranath Lo and Debashree Manna

Received: 30 December 2021
Accepted: 8 February 2022
Published: 15 February 2022

Publisher's Note: MDPI stays neutral with regard to jurisdictional claims in published maps and institutional affiliations.

Copyright: © 2022 by the authors. Licensee MDPI, Basel, Switzerland. This article is an open access article distributed under the terms and conditions of the Creative Commons Attribution (CC BY) license (https://creativecommons.org/licenses/by/4.0/).

1. Introduction

Over the past few decades, the environment has been heavily filling with toxic, inflammable, and harmful gases due to the unceasing development of industries and deforestation [1]. The level of these gases has been excessively increasing in the atmosphere since industrialization. For a safe and healthy environment, the detection of these gases is required [2–4]. The need for an effective gas sensor is then extremely important. Numerous gas sensors based have been developed including the IDE (interdigitated electrode) [5–7], FET (field-effect transistor) [8,9], MEMS (microelectromechanical systems) [10,11], and QCM [12–14]. Among them, the QCM-based gas sensor is very effective owing to its beneficial features including accuracy, high sensitivity, and fast response. Also, QCM can be easily integrated with other electronic components [15,16].

In these gas sensors, metal oxide semiconductors, such as zinc oxide (ZnO) [17], nickel oxide (NiO) [18], tin oxide (SnO_2) [19,20], titanium dioxide (TiO_2) [21], and copper oxide (CuO) [22], have been used as the sensing materials. Among numerous metal oxide semiconductors, CuO has gained more attention due to its low cost, non-toxicity, facile preparation, and high surface reactivity [23,24]. CuO is a p-type semiconductor and has a narrow bandgap of 1.2–1.9 eV and exhibits excellent properties that have been utilized in a number of applications such as electrode materials for lithium-ion batteries, thin-film electrodes [25,26], catalysts [21], and gas sensors [27]. However, these CuO sensing materials need a high temperature to operate, which limits its gas sensing capability at room temperature.

The incorporation of CuO with carbon-based materials can be effective in the development of reliable gas sensors at room temperature (RT). A carbon-based two-dimensional (2D) material like graphene has outstanding electronic, mechanical, and thermal properties as well as a large surface-to-volume ratio [28–30]. Graphene has been used as a sensing material for RT detection of various gases, such as nitrogen dioxide (NO_2), sulfur dioxide (H_2S), ammonia (NH_3), and hydrogen (H_2) [31–35], but the lower electrical conductivity of graphene thin-films limits the ability of these sensors to achieve high performance.

Here, we report a CuO/functionalized graphene (rGO) hybrid nanostructure as a promising sensing material for QCM-based sensors for detecting gas at room temperature. To the best of our knowledge, a CuO/rGO-hybrid coated QCM sensor has not been previously reported. The CuO/rGO hybrid has not been discussed systematically on a QCM sensor for gas sensing applications. In summary, initially, the CuO nanoparticles (NPs) are prepared using copper acetate as a precursor and are then mixed with a functionalized graphene oxide solution. The functionalized graphene oxide solution is obtained using a chemical reduction method with ascorbic acid. The sensing thin-films of the synthesized hybrid material are developed by the drop-cast method. The synergistic effect of CuO and graphene in the hybrid structure can help achieve the detection of gas at room temperature. The CuO/rGO hybrid offers beneficial properties such as enhanced surface reactivity, good electrical conductivity, and a large surface area. In this study, the CuO/rGO hybrid and rGO-based gas sensors are investigated for CO_2 gas sensing capability at room temperature.

2. Materials and Methods

2.1. Materials

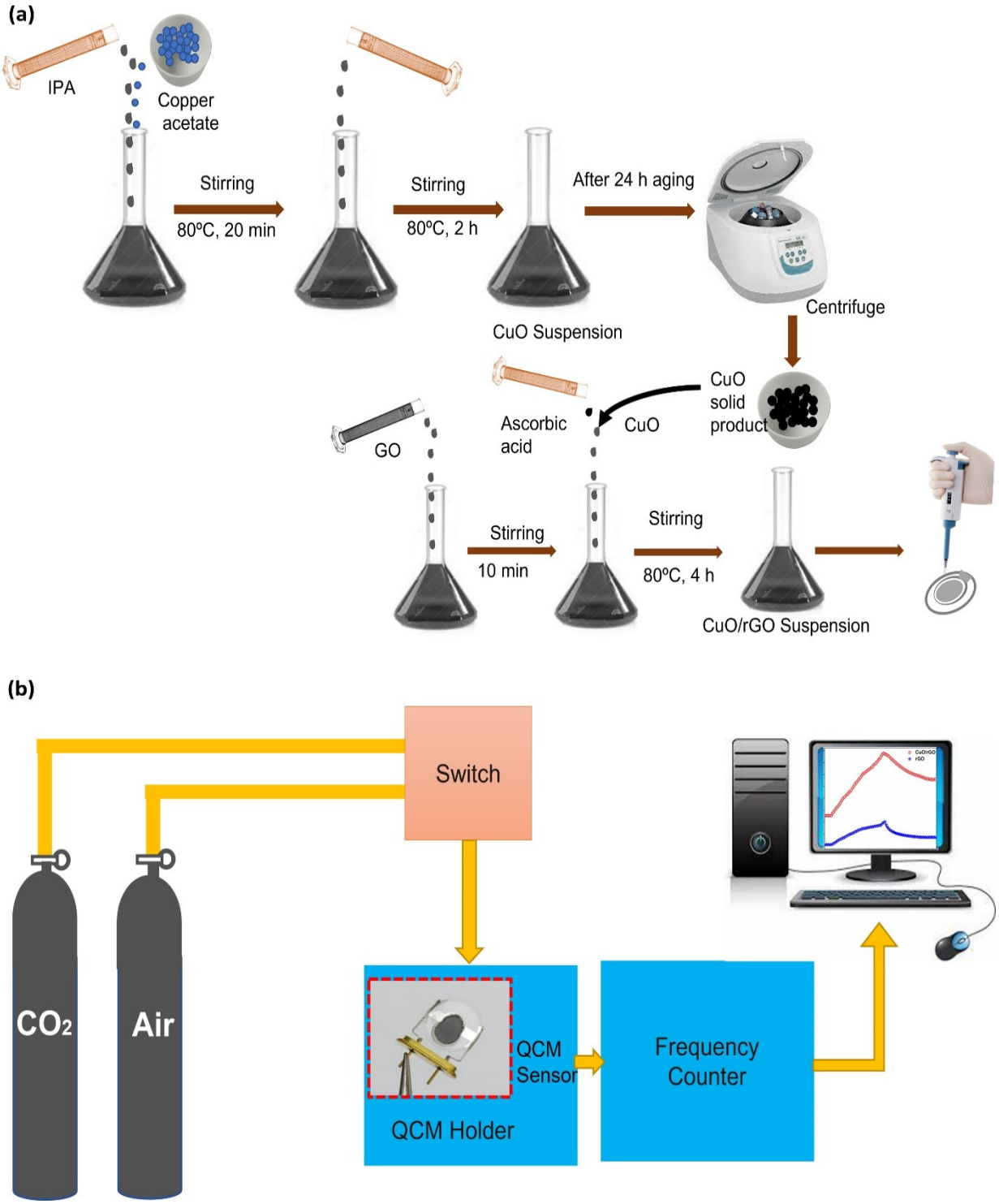
Graphene oxide (GO) paste (95%) was purchased from Graphenea (San Sebastian, Spain). Ascorbic acid, ethanol (95%), and acetone (95%) were purchased from Sigma-Aldrich (St. Louis, MO, USA). Copper acetate (99.9% purity), hexamethylenetetramine, and isopropyl alcohol (IPA, 99.9% purity) were bought from R & M Chemicals, Selangor, Malaysia. All the chemicals were of analytical grade, no further purification was required for conducting the experiments. Deionized (DI) water was used in all preparations.

2.2. Synthesis of CuO/Functionalized Graphene Hybrid and Thin-Film Development

The schematic representation of (a) the sensing material and thin-film development and (b) gas sensing set-up is shown in Scheme 1. Initially, 4 g of copper acetate is added to 60 mL IPA and mixed under stirring conditions at 80 °C for 20 min. Then, 4 mL of ethanolamine (MEA) is added carefully to the solution and stirred vigorously for 2 h. The prepared solution is left for 24 h for aging. The solution is further washed with water and the solid product is separated using centrifugation. Next, 30 mL graphene oxide (0.5 mg/mL) is dissolved in 100 mL of DI water and vigorously stirred for 10 min to form a well-mixed suspension. Then, 100 mg ascorbic acid (AA) is carefully added to the suspension. Afterward, 0.02 g of obtained CuO powder is added immediately to this GO suspension followed by vigorous stirring at 80 °C for 4 h. The suspension is further washed with ethanol and water (1:1 ratio). The solid product is later collected after the centrifugation followed by drying in an oven at 60 °C.

For comparison, the rGO is synthesized according to our previous work [36]. In brief, 15 mL of GO is added to 30 mL of DI water followed by ultrasonication for 15 min to acquire a uniform aqueous dispersion. Then, 100 mg of ascorbic acid is carefully added to the GO suspension, then stirred for 1 h at 65 °C under RT conditions. The change in color of the GO suspension from brown to black suggests the functionalized graphene oxide has been obtained.

The thin films of synthesized rGO suspensions and CuO/rGO hybrid are developed by the drop-casting method. Before thin-film development, target substrates such as glass and SiO_2 (300 nm)/Si are washed in acetone, isopropyl alcohol, DI water, and ethanol using ultrasonication for 15 min for each solvent.



Scheme 1. Schematic representation of (**a**) sensing material and the thin-film development (**b**) gas sensing set-up with developed CuO/rGO gas sensor (inset).

For sensor fabrication, thin sensing layers of the CuO/rGO hybrid and rGO materials are dropcast on a silver (Ag) electrode of 10 MHz QCM (WTL International China, Shenzhen, China). Before that, the QCM resonators are cleaned properly using acetone, isopropyl alcohol (IPA), DI water, and ethanol. A custom-made QCM based gas-sensing setup is used to obtain the sensing performance. Before sensing, the rGO and CuO/rGO-coated QCM are dried at room temperature.

2.3. Characterization

The structural and morphological properties of synthesized materials were investigated by Fourier Transform Infrared (FTIR) spectroscopy (Bruker Instruments, Model Aquinox 55, Stuttgart, Germany), Raman spectroscopy (Horiba Jobin Yvon HR800, Yvon, France, 514 nm laser excitation) for 200 to 4000 cm^{-1} spectrum regions, and transmission electron microscopy (TEM, Zeiss Libra 200FE, Jena, Germany), respectively. The sheet resistance of thin-films of prepared materials was measured using a four-point probe measurement system (Lucas Lab 302) with a Keithley 2400 source meter.

For investigating the gas sensing properties, a custom made QCM-based gas sensing setup was used for the experiments at room temperature. For the gas sensing experiment, rGO and the CuO/rGO-hybrid coated QCMs were placed inside the QCM holder. In the typical arrangement, the QCM holder is connected to the frequency counter. Firstly the air was purged onto the rGO and CuO/rGO-coated QCM sensor for 50 s, then the gas was purged onto the rGO and CuO/rGO-coated QCM sensors for 50 s at room temperature. The analyte gas molecules were absorbed at the material surface and the frequency of QCM was changed. The frequency counter measured the frequency change. The rGO and the hybrid-coated QCM sensors were again exposed to air to desorb the analyte gas molecule from its surface. The response and recovery curve was observed in real-time on the connected computer. The mass sensitivity, S_m (Hz/μg) was assessed by frequency shift/amount of coating material, to compare the material performance. The sensor sensitivity, Sg (Hz/ppm), was calculated as frequency shift/gas, in ppm [13,37,38].

3. Results and Discussion

3.1. FTIR Analysis

FTIR spectrum is used to identify the presence of functional groups and chemical compounds. The FTIR spectra of GO, rGO, and the CuO/rGO hybrid are shown in Figure 1. The FTIR spectrum of GO exhibited strong peaks at 3182 cm^{-1}, 1620 cm^{-1}, and 1044 cm^{-1}, which was attributed to the stretching and deformation of -OH and -COOH functional groups, as well as the adsorbed and inhibited water molecules to atmospheric moisture [39,40]. The peaks at 1724 cm^{-1} and 1620 cm^{-1} were the vibrations of the C=O and C=C alkene groups. Some other peaks at 1225 cm^{-1} and 1044 cm^{-1} were also observed, indicating the presence of the C–O stretching vibration of epoxy groups and an alkoxy group, respectively. Also, in the rGO spectra, weak peaks at 2322 cm^{-1} and 1391 cm^{-1} were observed, possibly due to the stretching and deformation of O–H groups and adsorbed water molecules, respectively. The spectrum of rGO also indicated the presence of stretching vibration bands for C=O at 1717 cm^{-1} and C–O for epoxy and alkoxy at 1219 cm^{-1} and 1007 cm^{-1}, respectively.

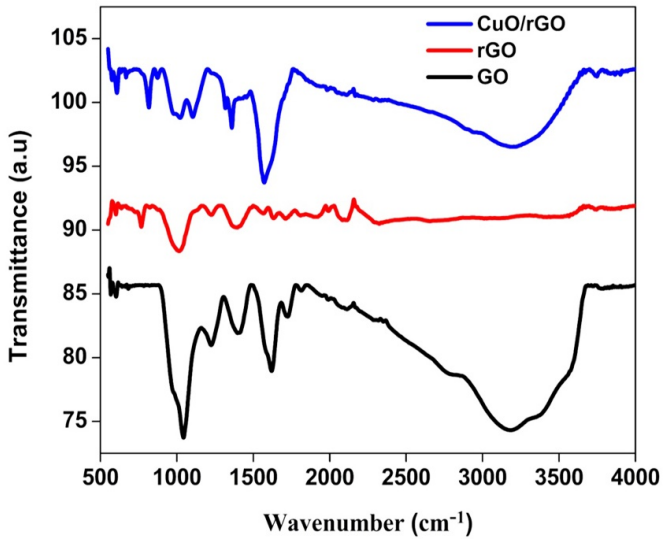


Figure 1. FTIR spectra of GO, rGO, and the CuO/rGO hybrid.

After the formation of the CuO/rGO hybrid, the peaks for the functional group were found to be shifted to 3198 cm^{-1} (hydroxyl), 1570 cm^{-1} (carboxyl), and 1023 cm^{-1} (epoxy). This suggests that the oxygen functional groups (OFGs), particularly hydroxyls, emerged during the formation of the hybrid nanostructure. However, a weak peak for hydroxyls was found in the rGO nanostructure. In the CuO/rGO hybrid spectrum, some additional peaks at 560 cm^{-1}, 576 cm^{-1}, and 607 cm^{-1} were also observed, identifying the vibrations of the Cu–O bond [41]. The presence of these peaks was also attributed to the stabilization of CuO nanoparticles through the residual OFGs present in rGO and indicated the presence of copper nanoparticles along with rGO [42].

3.2. Raman Analysis

The Raman spectrum of the CuO/rGO hybrid is presented in Figure 2 and compared with the spectra of GO and rGO. The D-peaks for GO, rGO, and the CuO/rGO hybrid were found at the Raman shift of ~1355 cm^{-1}, ~1353 cm^{-1}, and 1350 cm^{-1}, respectively. The G-peaks for GO, rGO, and the CuO/rGO hybrid were observed at the Raman shift of ~1586 cm^{-1}, 1600 cm^{-1}, and 1594 cm^{-1}, respectively (see Figure 3a). Typically, the D-peak appears from the defects in sp^3 carbon atoms whereas the G-peak correlates to the sp^2 carbon atoms [43,44]. The prepared rGO and CuO/rGO material inhibited intense D-peaks and G-peaks, which was attributed to the presence of defects in the graphene layer. The D-peak of rGO and the CuO/rGO hybrid was observed to be more intense as compared to G-peak, indicating the formation of sp^3 graphitic domains and the formation of new defects in the structure during the reduction process [39,45]. The occurrence of two additional peaks at a low-frequency Raman shift of ~322 cm^{-1} and ~678 cm^{-1}, was identified as the A_g and B_g modes of the vibration of CuO, respectively [46]. The 2D peaks were observed at ~2679 cm^{-1}, ~2689 cm^{-1}, and ~2701 cm^{-1} for GO, rGO, and the CuO/rGO hybrid, respectively. The 2D band also known as the G′-band, originated from the second-order mode of the D-band [47]. The higher wavenumber position and the lower peak height of the 2D-band of the CuO/rGO hybrid suggest the existence of more graphene layers compared to rGO. Moreover, it indicates that the CuO nanoparticles located between the graphene layers work as a spacer to hinder the agglomeration of graphene layers.

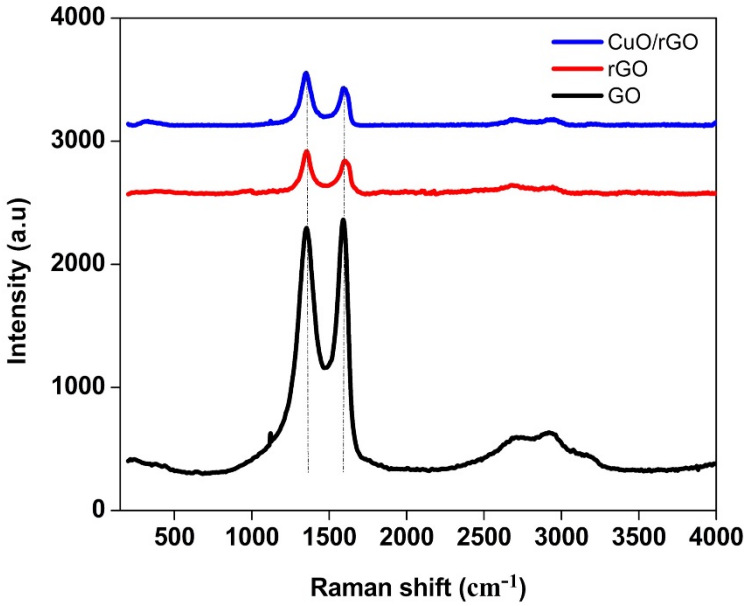


Figure 2. Raman spectra of the CuO/rGO hybrid, rGO, and GO.

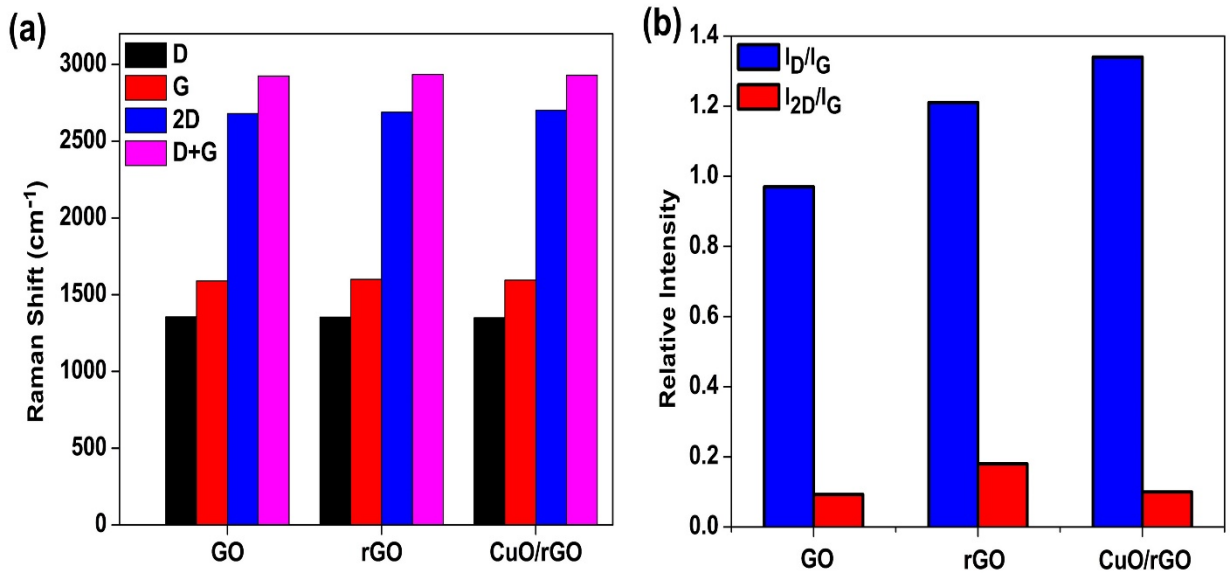


Figure 3. Raman fingerprints: (**a**) position of D-, G-, 2D-, and D + G-peaks, (**b**) average values of the parameters I_D/I_G, I_{2D}/I_G obtained from the Raman Spectra of rGO and the CuO/rGO hybrid.

The I_D/I_G intensity ratio (see Figure 3b) was found to be 0.97, 1.21, and 1.35 for GO, rGO, and the CuO/rGO hybrid, respectively. The I_D/I_G ratio represents the quality or disorder level of graphene. The relatively high value of I_D/I_G for the CuO/rGO hybrid suggests the formation of higher graphitic domains (smaller spatial dimensions) [48]. This indicates a decrease in the average size of the sp^2 carbon domain upon the reduction of GO. Similar results were also reported by Cheng et al. [49]. The higher intensity of the D-peak shows the presence of a large amount of OFGs that are favorable for the physisorption of analyte gas molecules. Reduced graphene oxide consists of graphene layers and OFGs attached at its basal plane and edges [39]. The I_{2D}/I_G ratios for GO, rGO, and the CuO/rGO hybrid were found to be 0.093, 0.18, and 0.13 indicating the presence of a few layers of graphene in the CuO/rGO hybrid.

The deconvoluted Raman spectra (Lorentz fit) of GO, rGO, and the CuO/rGO hybrid are shown in Figure 4. The heights of the D-band, G-band, 2D-band, and D+G-band are shown in Table 1. It was observed that the intensity of the D-peak of rGO and the CuO/rGO hybrid were lower than the D-peak of GO, which was attributed to the presence of fewer OFGs in the rGO and CuO/rGO hybrid material. Also, the intensity of the G-peak was found to be lower than that of the D-peak in rGO and the hybrid material, showing that these materials have higher defects [50,51].

Full width half maximum (FWHM) values of D- and G-peaks of GO, rGO, and the CuO/rGO hybrid are shown in Table 2. A lower value of FWHM of the D- and G-bands for the CuO/rGO hybrid (~81 cm^{-1} and ~60 cm^{-1}) and rGO (~76 cm^{-1} and 288 cm^{-1}) in comparison to GO (~153 cm^{-1} and 75 cm^{-1}) indicates the presence of fewer OFGs in their structures.

Table 1. Intensity (a.u.) of the bands in the Raman spectra of GO, rGO, and the CuO/rGO hybrid.

Sample	D-Band	G-Band	2D-Band	D + G
GO	1877	1947	181	273
rGO	321	265	48	32
CuO/rGO	411	305	41	43

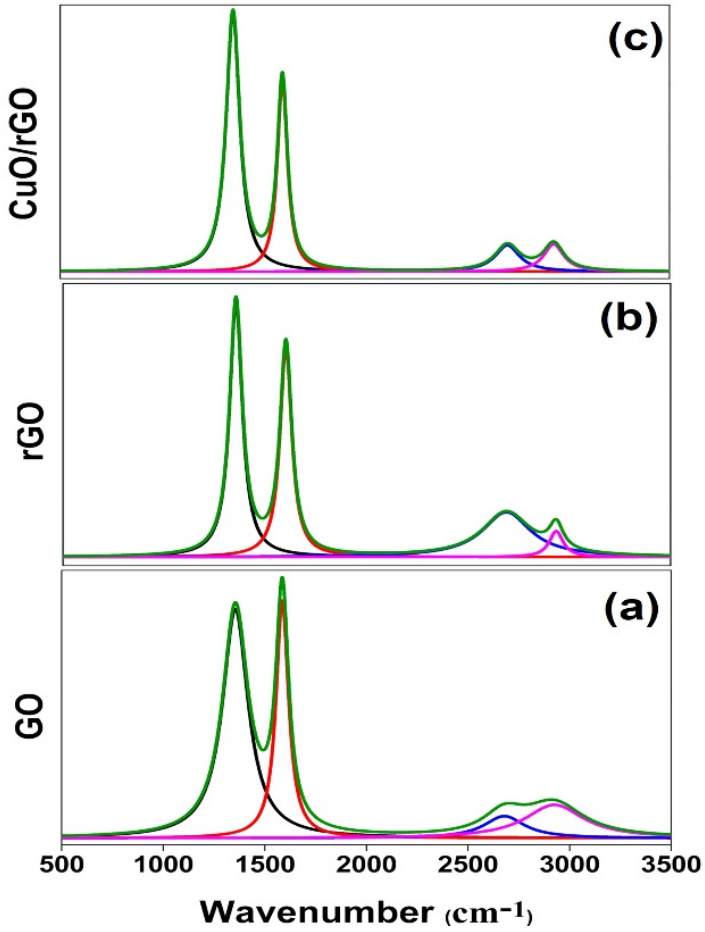


Figure 4. Deconvoluted (Lorentz fit) Raman curve of GO, rGO, and the CuO/rGO hybrid.

Table 2. FWHM (cm^{-1}) values of the bands in the Raman spectra of GO, rGO, and the CuO/rGO hybrid.

Sample	D-Band	G-Band	2D-Band	D + G
GO	153	75	241	350
rGO	76	288	82	82
CuO/rGO	81	60	146	120

3.3. SEM and TEM Analysis

The structure and morphology of the synthesized materials can be studied using SEM and TEM. Figure 5a shows the SEM image of rGO, which consists of wrinkles on its surface. Figure 5b shows the surface of the CuO/rGO hybrid, wherein the CuO NPs are distributed throughout the graphene sheets.

Figure 5c shows the TEM-based rGO morphology. The surface of rGO was identified as a continuous thin layer with a few folds and wrinkles on the edges of rGO sheets. Figure 5d shows the surface morphology of the CuO/rGO hybrid wherein CuO, in the form of nanoparticles, was well-mixed with rGO. The size (diameter) of the CuO particles was observed in the range of 10–40 nm. The CuO nanoparticles were observed to be randomly distributed on the basal plane of the rGO sheets, providing enough surface contact for charge transport. The inset shows the high-resolution image of the CuO/rGO hybrid, displaying the 35 nm CuO nanoparticles on the rGO sheets.

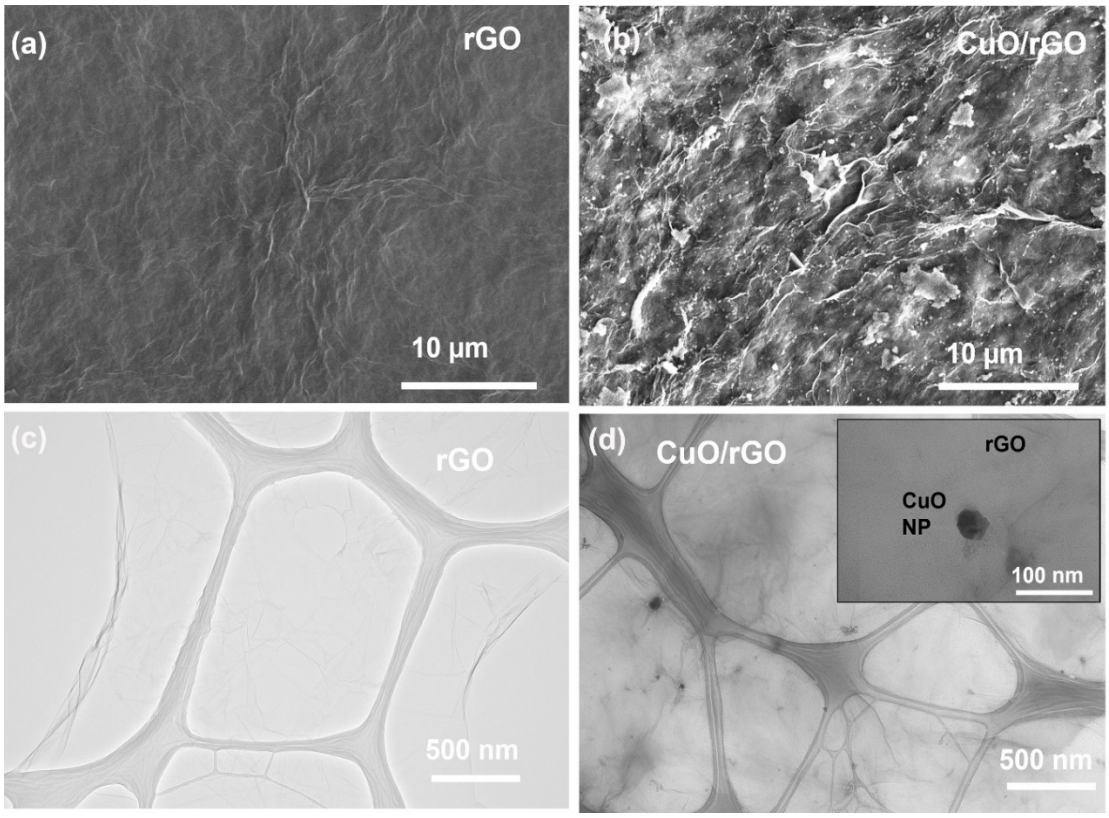


Figure 5. SEM image of (**a**) rGO, and (**b**) the CuO/rGO hybrid; TEM images of (**c**) rGO, and (**d**) the CuO/rGO hybrid. A high-resolution image of the hybrid is shown in the inset.

3.4. Electrical Analysis

Figure 6 shows the sheet resistance (R_S) of the rGO and the CuO/rGO hybrid thin-films. To investigate the electrical properties of the materials a four-point probe technique was used. The electrical characterization was carried out at room temperature. The R_S of rGO and the CuO/rGO hybrid was found to be 1.85 ± 0.12 kΩ/□ and 1.665 ± 0.11 kΩ/□, respectively. The lower sheet resistance of the hybrid was probably due to the presence of CuO nanoparticles.

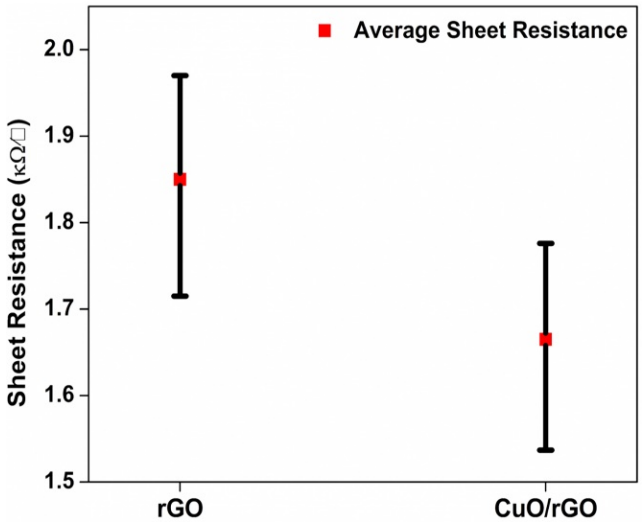


Figure 6. The sheet resistance of rGO and the CuO/rGO hybrid thin-films.

3.5. Gas Sensing Performance

Figure 7a,b shows the response and recovery curves of rGO and the CuO/rGO thin-film based QCM gas sensors for 50 and 500 ppm CO_2 at room temperature. A frequency shift (Δf) of 438 Hz was shown by the gas sensor with the rGO/CuO hybrid sensing thin-film whereas, a Δf of 193 Hz was demonstrated by rGO thin-film based sensor. The higher response of the hybrid sensing film was possibly due to the presence of more OFGs at its surface as indicated by the FTIR spectra. Also, due to incorporation of CuO nanoparticles between the graphene layers the effective surface area was increased, which resulted in a better response for hybrid. The CO_2 gas was also exposed to the GO-coated QCM sensor at RT. The prepared GO-coated QCM sensor showed no response upon CO_2 gas exposure possibly due to the unavailability of active sites on its surface. GO has mainly hydroxyl and epoxide groups at its basal plane and it loses sp^2 hybridization during the oxidation process which makes GO an insulating material at room temperature [39].

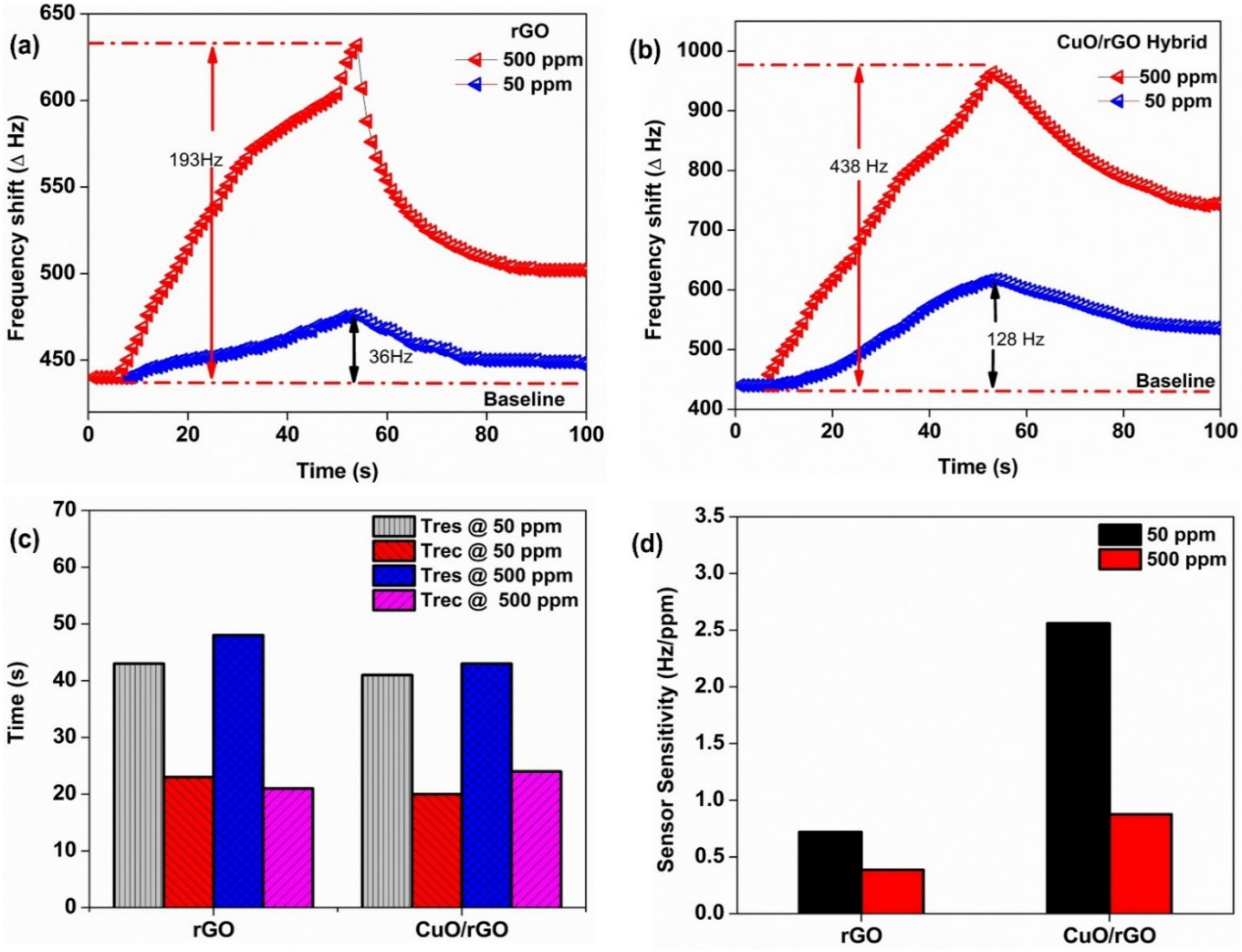


Figure 7. The sensing response curve of QCM gas sensors with (**a**) rGO, and (**b**) the CuO/rGO hybrid. Comparison of (**c**) response time (s), recovery time (s) and (**d**) sensitivity (Hz/μg) of rGO and the CuO/rGO hybrid-based gas sensors for 50 ppm and 500 ppm CO_2 gas.

The comparison between the response time (T_{res}) and the recovery time (T_{rec}) of rGO and the CuO/rGO hybrid-based gas sensors is presented in Figure 7c. The response time (T_{res})/recovery time (T_{rec}) was observed to be 43 s/23 s for rGO, and 41 s/20 s for the CuO/rGO hybrid for 50 ppm. The T_{res}/T_{rec} was found to be 48 s/21 s for rGO, and 43 s/24 s for the CuO/rGO hybrid for 500 ppm. The CuO/rGO hybrid–based sensor showed more

recovery time than that of the rGO-based sensor. This was possibly due to the formation of hydroxyl groups. The gas sensing characteristics, frequency shift, response time, and recovery time strongly depended on the interactions between the oxygen functional group (OFG) and the analyte gas molecule [12,52]. The hybrid required a higher time to recover due to the formation of hydroxyl bonds. Hydroxyl bonds were mainly attached to the basal plane however carboxyls and carbonyls were mainly attached to the edge plane of the graphene [39]. These hydroxyls worked as trap charges for the analyte gas molecule. Although the rGO and CuO/rGO hybrid thin-film based sensors showed a good response towards CO_2 gas, both sensors demonstrated baseline drift because the adsorbed CO_2 molecules did not desorb completely during the desorption process.

The sensor sensitivity comparison is shown in Figure 7d. The sensor sensitivity of the rGO-coated QCM sensor was found to be 0.72 Hz/ppm for 50 ppm and 0.386 Hz/ppm for 500 ppm CO_2 gas, and the CuO/rGO hybrid-coated QCM sensor was 2.56 Hz/ppm for 50 ppm and 0.876 Hz/ppm for 500 ppm. The mass sensitivity of the QCM sensors was also calculated and found to be 15 Hz/µg for the CuO/rGO-coated QCM sensor and 1 Hz/µg for the rGO-coated QCM sensor for 500 ppm, and 0.26 Hz/µg and 1.712 Hz/µg, respectively for 50 ppm. The performance comparison of various other material-coated QCM sensors are given in Table 3. The selectivity of the CuO/rGO-coated QCM sensor towards several volatile organic compounds (VOCs), such as ethanol, acetone, and toluene, was investigated. All the VOCs were measured at 500 ppm at room temperature. The magnitude of response of the VOCs is shown in Figure 8.

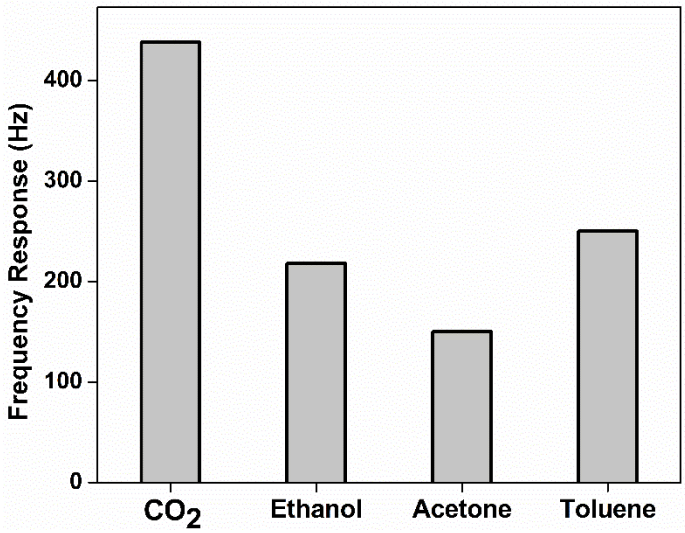


Figure 8. Comparison of the responses of the CuO/rGO hybrid-coated QCM sensor to 500 ppm of various gases/vapors.

The possible mechanism of the gas sensing by the CuO/rGO-coated QCM sensor is illustrated in Figure 9. First, the air was purged onto the CuO/rGO-coated QCM at room temperature. The oxygen molecules were adsorbed on the CuO/rGO hybrid surface by the physisorption process. Due to the CuO nanoparticles, the surface area of the hybrid increased which resulted in the absorption of more oxygen molecules. The concentration of oxygen molecules was increased due to the ionization of oxygen ions at the hybrid surface. The reaction process is shown below:

$$O_2(gas) \leftrightarrow O_2(ads) \quad (1)$$

$$O_2(ads) + e^- \leftrightarrow O_2^-(ads) \quad (2)$$

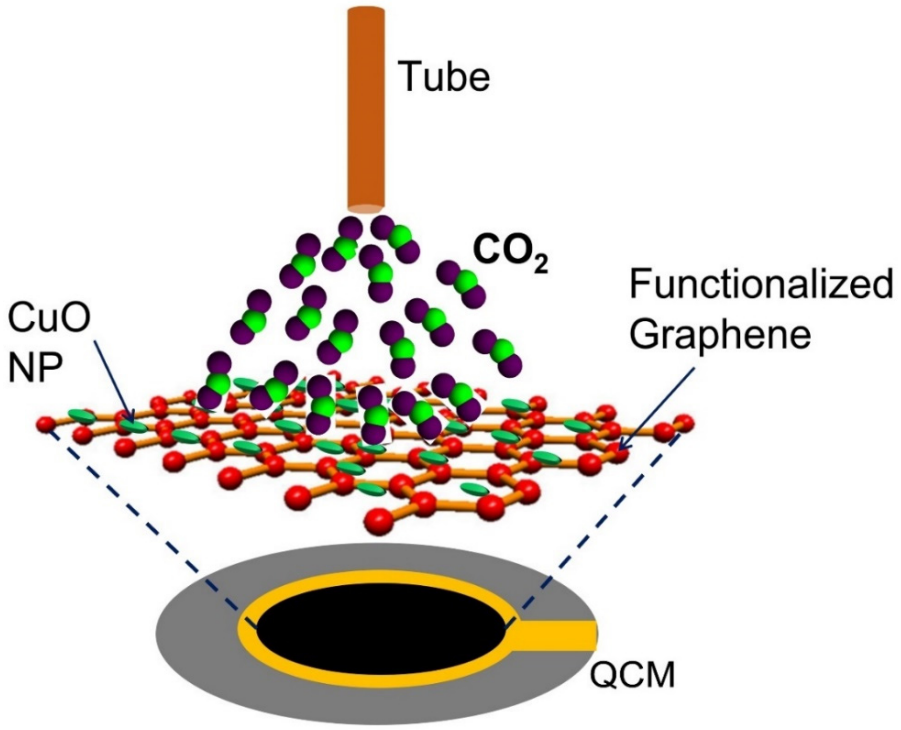


Figure 9. Schematic representation of analyte gas molecule adsorption on the CuO/rGO hybrid surface.

Then the analyte gas (CO_2) is flowed over the hybrid-coated QCM sensor surface, the oxygen ions interact with analyte gas molecules and form carbonate ions [12,53,54].

$$CO_2(gas) \leftrightarrow CO_2(ads) \tag{3}$$

$$2CO_2(gas) + O_2^- + e^- \rightarrow 2CO_3^-(ads) \tag{4}$$

Due to the adsorption of analyte gas, the concentration of the charge carrier is modulated at the hybrid surface. Therefore, the surface resistance is changed, depending on the sensing material and analyte gas (oxidizing/reducing gas).

Table 3. Performance comparison of various material-coated QCM sensors.

Materials	Synthesis Method	Detected Gas	Sensor Sensitivity (Hz/ppm)	Mass Sensitivity (Hz/μg)	Frequency Shift (Hz)/T_{res} (s)/T_{rec} (s)	References
graphene oxide/ TiO_2 composite	liquid phase deposition	ethanol	~0.925	-	370 Hz	[55]
citric acid monohydrate (CA) poly (ethylene glycol) diacrylate (CAPEGDA)	-	NH_3	~0.85	-	18 Hz/~5 min/~10 min	[56]
polyvinyl acetate (PVAc) nanofibers	electrospinning method	safrole	~1.866	~0.799	16.3 Hz/T_{res} = 171 s	[37]
vanadium Oxide	vacuum thermal evaporation	CO_2	-	-	50 s/125 s	[12]
cryptophane-A-based QCM sensor	electrospray method	CH_4, NO_2	0.103, 0.032	-	-	[57]
commercial CuO	hydrothermal treatment method	HCN	~0.82	~0.31	41 Hz/~300 s/~350 s	[13]
CuO/rGO hybrid	chemical synthesis	CO_2	2.56	15	438 Hz/~41 s/20 s	This work

4. Conclusions

In this work, we successfully synthesized the CuO/functionalized graphene hybrid material. The thin-films of material were developed by the drop-casting method on the substrates. The material properties were examined using advanced spectroscopy and microscopy. In the hybrid nanostructure, a wrinkled and folded graphene surface with randomly distributed CuO NPs of size 10–40 nm were observed. The hybrid material was also found to have a large amount of OFGs and defective sites on its surface. The

electrical conductivity of the CuO/rGO hybrid thin-film was measured to be ~1.5 kΩ/□. The functionality of the CuO/rGO hybrid was investigated as a sensing layer in the QCM sensor for gas detection at room temperature. The CuO/rGO hybrid-based gas sensor realized a high sensing response, Δf~440 Hz/T_{res}~43 s for 500 ppm and Δf~195 Hz/T_{res}~41 s for 50 ppm CO_2 gas at room temperature. The sensing performance of the CuO/rGO hybrid-based gas sensor was compared with that of the rGO-based sensor. A two-fold improved sensing response was achieved in comparison to the rGO-based sensor. The hybrid-coated QCM sensor also exhibited excellent selectivity towards CO_2 gas. This study shows the interesting possibilities of CuO/rGO hybrids in future gas sensing devices.

Author Contributions: Conceptualization, M.G. and H.F.H.; methodology, M.G. and P.K.; software, M.G.; formal analysis, M.G. and P.K.; investigation, M.G. and P.K.; resources, H.F.H.; data curation, M.G.; writing—original draft preparation, M.G.; writing—review and editing, P.K. and H.F.H.; visualization, M.G., P.K. and H.F.H.; supervision, H.F.H. and Z.A.B.; project administration, H.F.H.; funding acquisition, H.F.H. All authors have read and agreed to the published version of the manuscript.

Funding: This research was funded by Yayasan University of Technology PETRONAS (YUTP) grant (number: 015LC0-153). The publication charge was partially supported by the Center for Graduate Studies (CGS), UTP, Malaysia.

Data Availability Statement: The data are available upon request from the corresponding authors.

Acknowledgments: The authors would like to thank the graduate assistantship scheme from the CGS, UTP, Malaysia.

Conflicts of Interest: The authors declare no conflict of interest.

References

1. Leghrib, R. *Design, Fabrication and Characterisation of Gas Sensors Based on Nanohybrid Materials*; Universitat Rovira i Virgili: Tarragona, Spain, 2011.
2. Azuma, K.; Kagi, N.; Yanagi, U.; Osawa, H. Effects of low-level inhalation exposure to carbon dioxide in indoor environments: A short review on human health and psychomotor performance. *Environ. Int.* **2018**, *121*, 51–56. [CrossRef] [PubMed]
3. Yu, B.F.; Hu, Z.B.; Liu, M.; Yang, H.L.; Kong, Q.X.; Liu, Y.H. Review of research on air-conditioning systems and indoor air quality control for human health. *Int. J. Refrig.* **2009**, *32*, 3–20. [CrossRef]
4. Tanvir, N.B.; Yurchenko, O.; Wilbertz, C.; Urban, G. Investigation of CO_2 reaction with copper oxide nanoparticles for room temperature gas sensing. *J. Mater. Chem. A* **2016**, *4*, 5294–5302. [CrossRef]
5. Rathi, K.; Pal, K. Ruthenium decorated tungsten disulfide quantum dots for CO_2 gas sensor. *Nanot* **2019**, *31*, 135502. [CrossRef]
6. Daud, A.I.; Wahid, K.A.A.; Khairul, W.M. Room-temperature operated cyano-terminated ethynylated-thiourea as a resistive-type carbon dioxide (CO_2) gas sensor. *Org. Electron.* **2019**, *70*, 32–41. [CrossRef]
7. Young, S.-J.; Lin, Z.-D. Sensing Performance of Carbon Dioxide Gas Sensors with Carbon Nanotubes on Plastic Substrate. *ECS J. Solid State Sci. Technol.* **2017**, *6*, 72–74. [CrossRef]
8. Cui, S.; Pu, H.; Wells, S.A.; Wen, Z.; Mao, S.; Chang, J.; Hersam, M.C.; Chen, J. Ultrahigh sensitivity and layer-dependent sensing performance of phosphorene-based gas sensors. *Nat. Commun.* **2015**, *6*, 8632. [CrossRef]
9. Zhang, M.; Brooks, L.L.; Chartuprayoon, N.; Bosze, W.; Choa, Y.H.; Myung, N.V. Palladium/single-walled carbon nanotube back-to-back schottky contact-based hydrogen sensors and their sensing mechanism. *ACS Appl. Mater. Interfaces* **2014**, *6*, 319–326. [CrossRef]
10. Zia, A.I.; Syaifudin, A.R.M.; Mukhopadhyay, S.C.; Yu, P.L.; Al-Bahadly, I.H.; Gooneratne, C.P.; Kosel, J.; Liao, T.S. Electrochemical impedance spectroscopy based MEMS sensors for phthalates detection in water and juices. *J. Phys. Conf. Ser.* **2013**, *439*, 012026. [CrossRef]
11. Algamili, A.S.; Khir, M.H.M.; Dennis, J.O.; Ahmed, A.Y.; Alabsi, S.S.; Ba Hashwan, S.S.; Junaid, M.M. A Review of Actuation and Sensing Mechanisms in MEMS-Based Sensor Devices. *Nanoscale Res. Lett.* **2021**, *16*, 16. [CrossRef]
12. Berouaken, M.; Talbi, L.; Alkama, R.; Sam, S.; Menari, H.; Chebout, K.; Manseri, A.; Boucheham, A.; Gabouze, N. Quartz Crystal Microbalance Coated with Vanadium Oxide Thin Film for CO_2 Gas Sensor at Room Temperature. *Arab. J. Sci. Eng.* **2018**, *43*, 5957–5963. [CrossRef]
13. Yang, M.; He, J.; Hu, X.; Yan, C.; Cheng, Z. CuO nanostructures as quartz crystal microbalance sensing layers for detection of trace hydrogen cyanide gas. *Environ. Sci. Technol.* **2011**, *45*, 6088–6094. [CrossRef] [PubMed]
14. Vashist, S.K.; Vashist, P. Recent advances in quartz crystal microbalance-based sensors. *J. Sens.* **2011**, *2011*, 571405. [CrossRef]
15. Varga, M.; Laposa, A.; Kulha, P.; Kroutil, J.; Husak, M.; Kromka, A. Quartz crystal microbalance gas sensor with nanocrystalline diamond sensitive layer. *Phys. Status Solidi Basic Res.* **2015**, *252*, 2591–2597. [CrossRef]

16. Gupta, M.; Athirah, N.; Hawari, H.F. Graphene derivative coated QCM-based gas sensor for volatile organic compound (VOC) detection at room temperature. *Indones. J. Electr. Eng. Comput. Sci.* **2020**, *18*, 1279–1286. [CrossRef]
17. Zhu, B.L.; Xie, C.S.; Wang, W.Y.; Huang, K.J.; Hu, J.H. Improvement in gas sensitivity of ZnO thick film to volatile organic compounds (VOCs) by adding TiO_2. *Mater. Lett.* **2004**, *58*, 624–629. [CrossRef]
18. Ren, H.; Gu, C.; Joo, S.W.; Zhao, J.; Sun, Y.; Huang, J. Effective hydrogen gas sensor based on NiO@rGO nanocomposite. *Sens. Actuators B Chem.* **2018**, *266*, 506–513. [CrossRef]
19. Chen, W.; Zhou, Q.; Wan, F.; Gao, T. Gas sensing properties and mechanism of Nano-SnO2-based sensor for hydrogen and carbon monoxide. *J. Nanomater.* **2012**, *2012*, 612420. [CrossRef]
20. Lee, Z.Y.; Hawari, H.F.B.; Djaswadi, G.W.B.; Kamarudin, K. A highly sensitive room temperature CO_2 gas sensor based on sno2-rgo hybrid composite. *Materials* **2021**, *14*, 522. [CrossRef]
21. Yuan, J.; Zhang, J.-J.; Yang, M.-P.; Meng, W.-J.; Wang, H.; Lu, J.-X. CuO Nanoparticles Supported on TiO_2 with High Efficiency for CO_2 Electrochemical Reduction to Ethanol. *Catalysts* **2018**, *8*, 171. [CrossRef]
22. Bhuvaneshwari, S.; Gopalakrishnan, N. Facile synthesis of low dimensional CuO nanostructures and their gas sensing applications. *Cryst. Res. Technol.* **2016**, *51*, 145–153. [CrossRef]
23. Purushothaman, K.K.; Saravanakumar, B.; Babu, I.M.; Sethuraman, B.; Muralidharan, G. Nanostructured CuO/reduced graphene oxide composite for hybrid supercapacitors. *RSC Adv.* **2014**, *4*, 23485–23491. [CrossRef]
24. Nagaraja, M.; Prashanth, S.; Pattar, J.; Mahesh, H.M.; Rajanna, K. Polyaniline-CuO nanocomposite: Electrical, structural and sensor properties. *Mater. Today Proc.* **2022**, *49*, 1989–1992. [CrossRef]
25. Kumar, P.; Kang, C.H.; Burhanudin, Z.A.; Saheed, M.S.M.; Irshad, M.I.; Mohamed, N.M. Graphene-based hybrid thin films as transparent conductive electrode for optoelectronic devices. In Proceedings of the IEEE International Conference on Semiconductor Electronics, Kuala Lumpur, Malaysia, 17–19 August 2016; Volume 2016, pp. 216–219.
26. Kondee, S.; Arayawut, O.; Pon-On, W.; Wongchoosuk, C. Nitrogen-doped carbon oxide quantum dots for flexible humidity sensor: Experimental and SCC-DFTB study. *Vacuum* **2022**, *195*, 110648. [CrossRef]
27. Mandayo, G.G.; González, F.; Rivas, I.; Ayerdi, I.; Herrán, J. $BaTiO_3$-CuO sputtered thin film for carbon dioxide detection. *Sens. Actuators B Chem.* **2006**, *118*, 305–310. [CrossRef]
28. Yoon, H.J.; Jun, D.H.; Yang, J.H.; Zhou, Z.; Yang, S.S.; Cheng, M.M.C. Carbon dioxide gas sensor using a graphene sheet. *Sens. Actuators B Chem.* **2011**, *157*, 310–313. [CrossRef]
29. Macinnes, M.M.; Hlynchuk, S.; Acharya, S.; Lehnert, N.; Maldonado, S. Reduction of Graphene Oxide Thin Films by Cobaltocene and Decamethylcobaltocene. *ACS Appl. Mater. Interfaces* **2018**, *10*, 2004–2015. [CrossRef]
30. Lesiak, B.; Trykowski, G.; Tóth, J.; Biniak, S.; Kövér, L.; Rangam, N.; Stobinski, L.; Malolepszy, A. Chemical and structural properties of reduced graphene oxide—dependence on the reducing agent. *J. Mater. Sci.* **2021**, *56*, 3738–3754. [CrossRef]
31. Ayesh, A.I.; Ahmed, R.E.; Al-Rashid, M.A.; Alarrouqi, R.A.; Saleh, B.; Abdulrehman, T.; Haik, Y.; Al-Sulaiti, L.A. Selective gas sensors using graphene and CuO nanorods. *Sens. Actuators A Phys.* **2018**, *283*, 107–112. [CrossRef]
32. Guo, L.; Hao, Y.W.; Li, P.L.; Song, J.F.; Yang, R.Z.; Fu, X.Y.; Xie, S.Y.; Zhao, J.; Zhang, Y.L. Improved NO_2 Gas Sensing Properties of Graphene Oxide Reduced by Two-beam-laser Interference. *Sci. Rep.* **2018**, *8*, 4918. [CrossRef]
33. Sharma, B.; Kim, J.S. MEMS based highly sensitive dual FET gas sensor using graphene decorated Pd-Ag alloy nanoparticles for H_2 detection. *Sci. Rep.* **2018**, *8*, 5902. [CrossRef] [PubMed]
34. Hu, N.; Yang, Z.; Wang, Y.; Zhang, L.; Wang, Y. Ultrafast and sensitive room temperature NH_3 gas sensors based on chemically reduced graphene oxide. *Nanotechnology* **2013**, *25*, 025502. [CrossRef] [PubMed]
35. Chaloeipote, G.; Samarnwong, J.; Traiwatcharanon, P.; Kerdcharoen, T.; Wongchoosuk, C. High-performance resistive humidity sensor based on Ag nanoparticles decorated with graphene quantum dots. *R. Soc. Open Sci.* **2021**, *8*, 210407. [CrossRef] [PubMed]
36. Gupta, M.; Hawari, H.F.; Kumar, P.; Burhanudin, Z.A.; Tansu, N. Functionalized reduced graphene oxide thin films for ultrahigh CO_2 gas sensing performance at room temperature. *Nanomaterials* **2021**, *11*, 623. [CrossRef] [PubMed]
37. Triyana, K.; Rianjanu, A.; Nugroho, D.B.; As'ari, A.H.; Kusumaatmaja, A.; Roto, R.; Suryana, R.; Wasisto, H.S. A highly sensitive safrole sensor based on polyvinyl acetate (PVAc) nanofiber-coated QCM. *Sci. Rep.* **2019**, *9*, 15407. [CrossRef] [PubMed]
38. Zhang, K.; Hu, R.; Fan, G.; Li, G. Graphene oxide/chitosan nanocomposite coated quartz crystal microbalance sensor for detection of amine vapors. *Sens. Actuators B Chem.* **2017**, *243*, 721–730. [CrossRef]
39. Yang, H.; Li, J.S.; Zeng, X. Correlation between molecular structure and interfacial properties of edge or basal plane modified graphene oxide. *ACS Appl. Nano Mater.* **2018**, *1*, 2763–2773. [CrossRef]
40. Kwan, Y.C.G.; Ng, G.M.; Huan, C.H.A. Identification of functional groups and determination of carboxyl formation temperature in graphene oxide using the XPS O 1s spectrum. *Thin Solid Films* **2015**, *590*, 40–48. [CrossRef]
41. Zhang, D.; Jiang, C.; Liu, J.; Cao, Y. Investigation of CO_2 reaction with copper oxide nanoparticles for room temperature gas sensing. *Sens. Actuators B Chem.* **2017**, *247*, 875–882. [CrossRef]
42. Singh, P.; Nath, P.; Arun, R.K.; Mandal, S.; Chanda, N. Novel synthesis of a mixed Cu/CuO-reduced graphene oxide nanocomposite with enhanced peroxidase-like catalytic activity for easy detection of glutathione in solution and using a paper strip. *RSC Adv.* **2016**, *6*, 92729–92738. [CrossRef]
43. Tang, Q.; Zhou, Z.; Chen, Z. Graphene-related nanomaterials: Tuning properties by functionalization. *Nanoscale* **2013**, *5*, 4541–4583. [CrossRef] [PubMed]

44. Zhang, Q.; Pang, X.; Zhao, Y. Effect of the external velocity on the exfoliation properties of graphene from amorphous SiO_2 surface. *Crystals* **2021**, *11*, 454. [CrossRef]
45. Bhaumik, A.; Haque, A.; Taufique, M.; Karnati, P.; Patel, R.; Nath, M.; Ghosh, K. Reduced Graphene Oxide Thin Films with Very Large Charge Carrier Mobility Using Pulsed Laser Deposition. *J. Mater. Sci. Eng.* **2017**, *6*, 1–11. [CrossRef]
46. Li, Z.; Liu, Y.; Guo, D.; Guo, J.; Su, Y. Room-temperature synthesis of CuO/reduced graphene oxide nanohybrids for high-performance NO_2 gas sensor. *Sens. Actuators B Chem.* **2018**, *271*, 306–310. [CrossRef]
47. Wu, J.B.; Lin, M.L.; Cong, X.; Liu, H.N.; Tan, P.H. Raman spectroscopy of graphene-based materials and its applications in related devices. *Chem. Soc. Rev.* **2018**, *47*, 1822–1873. [CrossRef]
48. Kumar, P.; Lin, K.; Seng, W.; Shuaib, M.; Saheed, M. Hybrid film of single-layer graphene and carbon nanotube as transparent conductive electrode for organic light emitting diode. *Synth. Met.* **2019**, *257*, 116186. [CrossRef]
49. Cheng, C.; Zhang, C.; Gao, X.; Zhuang, Z.; Du, C.; Chen, W. 3D Network and 2D Paper of Reduced Graphene Oxide/Cu_2O Composite for Electrochemical Sensing of Hydrogen Peroxide. *Anal. Chem.* **2018**, *90*, 1983–1991. [CrossRef]
50. Muzyka, R.; Drewniak, S.; Pustelny, T.; Chrubasik, M.; Gryglewicz, G. Characterization of graphite oxide and reduced graphene oxide obtained from different graphite precursors and oxidized by different methods using Raman spectroscopy. *Materials* **2018**, *11*, 1050. [CrossRef]
51. Wu, S.; Wan, L.; Wei, L.; Talwar, D.N.; He, K.; Feng, Z. Temperature-dependent optical properties of graphene on Si and SiO_2/Si substrates. *Crystals* **2021**, *11*, 358. [CrossRef]
52. Zaki, S.E.; Basyooni, M.A.; Shaban, M.; Rabia, M.; Eker, Y.R.; Attia, G.F.; Yilmaz, M.; Ahmed, A.M. Role of oxygen vacancies in vanadium oxide and oxygen functional groups in graphene oxide for room temperature CO_2 gas sensors. *Sens. Actuators A Phys.* **2019**, *294*, 17–24. [CrossRef]
53. Rodríguez-García, S.; Santiago, R.; López-Díaz, D.; Merchán, M.D.; Velázquez, M.M.; Fierro, J.L.G.; Palomar, J. Role of the Structure of Graphene Oxide Sheets on the CO_2 Adsorption Properties of Nanocomposites Based on Graphene Oxide and Polyaniline or Fe_3O_4-Nanoparticles. *ACS Sustain. Chem. Eng.* **2019**, *7*, 12464–12473. [CrossRef]
54. Shaban, M.; Ali, S.; Rabia, M. Design and application of nanoporous graphene oxide film for CO_2, H_2, and C_2H_2 gases sensing. *J. Mater. Res. Technol.* **2019**, *8*, 4510–4520. [CrossRef]
55. Jayawardena, S.; Siriwardena, H.D.; Rajapakse, R.M.G.; Kubono, A.; Shimomura, M. Fabrication of a quartz crystal microbalance sensor based on graphene oxide/TiO_2 composite for the detection of chemical vapors at room temperature. *Appl. Surf. Sci.* **2019**, *493*, 250–260. [CrossRef]
56. Liu, L.; Fei, T.; Guan, X.; Zhao, H.; Zhang, T. Highly sensitive and chemically stable NH_3 sensors based on an organic acid-sensitized cross-linked hydrogel for exhaled breath analysis. *Biosens. Bioelectron.* **2021**, *191*, 113459. [CrossRef] [PubMed]
57. Sun, P.; Jiang, Y.; Xie, G.; Du, X.; Hu, J. Sensors and Actuators B: Chemical A room temperature supramolecular-based quartz crystal microbalance (QCM) methane gas sensor. *Sens. Actuators B Chem.* **2009**, *141*, 104–108. [CrossRef]